Express Polymer Letters Vol.16, No.11 (2022) 1145–1160
Available online at www.expresspolymlett.com
https://doi.org/10.3144/expresspolymlett.2022.84

Research article

Compatibility, mechanical, and rheological properties of graphene oxide-containing ethylene-propylene-diene monomer (EPDM) compounds

*Natalia Garrote de Barros, Flavia Leticia Silva Freitas, Ticiane Sanches Valera**

Polytechnic School of the University of São Paulo (USP) Department of Metallurgical and Materials Engineering Av. Professor Mello Moraes, 2463, 05508-030 São Paulo, SP, Brazil

Received 10 April 2022; accepted in revised form 2 July 2022

Abstract. The interaction between reinforcing fillers and the elastomeric matrix determines the properties of the elastomeric nanocomposite. In this study, the properties of nanocomposites based on ethylene-propylene-diene monomer (EPDM) rubber compounds with graphene oxide (GO) and reduced GO (rGO) were investigated along with the effect of maleic anhydride (MAH) as a compatibilizing agent. GO- and rGO-containing nanocomposites were prepared using a combination of solution blending and torque rheometry processes. It was found that compositing with rGO reduced the optimal vulcanization times by approximately 5%. The addition of MAH improved the mechanical properties of the nanocomposites containing GO or rGO, with enhancements in elongation by 18 and 11% and in tensile strengths by 5 and 20%, respectively. The results showed good interactions between the nanoparticles and EPDM compounds. However, despite the good physicochemical affinity between MAH and GO, their simultaneous presence in the EPDM compound did not synergistically influence vulcanization and mechanical properties because of the excessive quantity of oxygen-containing functional groups present during the vulcanization process.

Keywords: *nanocomposites, reinforcement, rubber, maleic anhydride*

1. Introduction

The production of graphene-containing elastomeric nanocomposites has attracted attention for industrial applications that require improvements in mechanical, thermal, electrical, and gas barrier properties. Thus, the incorporation of graphene sheets and their derivatives in elastomers, such as ethylene-propylene-diene monomer (EPDM) rubber, has yielded a new class of nanocomposites showing combinations of their properties [1, 2]. EPDM is a polyolefin-type synthetic rubber with a highly saturated polymer backbone that can show improved mechanical properties with reinforcement. Owing to its excellent resistance to heat, oxidation, ozone, and weather aging, EPDM is widely used in outdoor electrical insulation and numerous automotive applications [3, 4].

Graphene is an atomically thick two-dimensional sheet composed of sp^2 carbon atoms arranged in a honeycomb structure [5]. Although it has excellent properties, its corresponding features are limited in nanocomposite applications owing to the issues of dispersion and interfacial interactions between the filler and polymer matrix [6].

One of the most widely used and commercially viable methods for the large-scale production of graphene is the production of graphene oxide (GO). The Brodie and Hummers methods for GO production have been extensively explored [7–9]. GO can be exfoliated into individual sheets in different solvents, resulting

*Corresponding author, e-mail: tsvalera@usp.br

in stable dispersions. This contributes to the homogenous incorporation of GO into an elastomer matrix as a reinforcing nanofiller, especially as the oxygen functional groups on the edges and surfaces of the graphene sheets convert some of the sp^2 carbon atoms to sp^3 [10, 11]. However, disadvantages during the oxidation process include the generation of defects and disorder in the crystal lattice of the GO sheets, which can yield different properties to the nanocomposites [12, 13].

For certain applications, especially those that require the recovery of electrical conductivity, it is desirable to restore the intrinsic properties of graphene by removing the oxygen functional groups from GO via a reduction process. Graphene undergoes considerable restacking during reduction owing to π–π and hydrophobic–hydrophobic interactions between the sheets, increasing the probability of agglomeration in the elastomer matrix. Therefore, the partial reduction of GO may benefit nanocomposite production owing to the remaining oxygen functional groups in the graphene sheets [14].

Methods for GO reduction have been described in the literature [13–16], with the purpose of completely or partially removing the oxygen-containing functional groups introduced during the oxidation of graphite to obtain GO. Chemical, thermal, electrochemical, biological, and photochemical reduction methods are commonly used. Thermal and chemical reductions are the most investigated procedures. However, both these methods have drawbacks. Thermal reduction is low in efficiency and can require high temperature and energy. Chemical reduction may generate impurities in the reduced GO (rGO) and involve the use of environmentally undesirable chemical compounds.

Electron beam irradiation (EBI) has recently been developed as a GO reducing technique. This method has been used for the synthesis and chemical modification of materials, and researchers [17, 18] have applied it to the reduction of GO. In this method, active free radicals with reduction potential (product of the radiolysis) are created to chemically react with GO and reduce it. The advantages of this method are its lack of chemical residues and its speed, efficiency, and scalability [17, 18].

Some studies [19–22] have demonstrated the effects of GO and rGO or other carbon-based materials on elastomers by analyzing the interactions between the matrix and filler and the vulcanization characteristics. Mensah *et al*. [19] compared the effects of GO and rGO reinforcement in EPDM and nitrile rubber (NBR) matrices and observed that the addition of graphene-based fillers modified the vulcanization and mechanical properties of the EPDM, even in a nonpolar EPDM matrix. Shanmugharaj *et al*. [21] showed that the addition of carbon-based fillers to natural rubber lowered vulcanization initiation temperatures in the presence of carboxylic acid groups and oxygen groups on the surface of the nanofillers, which could adsorb accelerator additives. In addition, Hernandez *et al*. [22] reported high thermal conductivity (5000 W/(m·K)) and high specific surface area (1850 m^2/g) of graphene sheets, which promoted the vulcanization reaction of natural rubber. Wu *et al*. [20] investigated more deeply the vulcanization steps of natural rubber and concluded that small amounts of GO (less than 1 phr) could modify the vulcanization kinetics. The induction period was decreased with the addition of low GO content, whereas the vulcanization time increased. Besides, these authors proposed that physical diffusion of the curing agents occurred, and the vulcanization reaction occurred in stages. The activation energy in the first stage decreased with the addition of GO, whereas an increase in activation energy was observed in the last, diffusion-controlled stage. Nevertheless, few studies on EPDM [19, 23, 24] have investigated the compatibility and influence of GO or rGO fillers in the vulcanization process.

It is known that nanocomposite properties strongly depend on nanofiller dispersion in the elastomer matrix. Many studies have focused on enhancing the dispersion of GO/rGO in polymers using solvents [1, 2, 25–27]. Kim *et al*. [1] investigated different mixtures to obtain nanocomposites of GO and thermoplastic polyurethane (TPU). The authors concluded that the solvent mixing technique was more effective than melting for dispersing reinforcing fillers. Dash *et al*. [28] prepared EPDM and graphene nanocomposites by solubilizing EPDM in toluene and exfoliating graphene in the same solvent. The Young's modulus increased from 0.045 to 1.24 MPa with 15% xGnP® (commercial graphene nanoplatelets), showing an improvement in mechanical properties with this dispersion method. Chen *et al*. [3] obtained nanocomposites by the combined methodology of solubilization and twin-screw mixing. The EPDM was dissolved in toluene, whereas GO was obtained using the Hummers method from ultrasonic exfoliation in

tetrahydrofuran (THF). After mixing and subsequent solvent extraction, the composite was mixed using a torque rheometer with a rotation of 60 rpm at room temperature. All the mechanical properties were improved, such as tensile stress (an increase of 52%) and elongation at break (an increase of 32%). Paredes *et al*. [10] and Konios *et al*. [11] investigated the dispersion behavior of GO and rGO in solvents. Paredes *et al*. [10] investigated the dispersion of GO produced by the Hummers method in organic solvents and verified that GO dispersions with long-term stability formed in water, dimethylformamide (DMF), n-methyl pyrrolidone (NMP), THF, and ethylene glycol. Both studies indicated that THF is a stable solvent for the dispersion of GO and rGO.

Although the use of certain solvents allows for good dispersion of GO, the use of compatibilizers can promote better dispersion and yield composites and nanocomposites with better mechanical properties. Modification with maleic anhydride (MAH) in different types of elastomers can induce compatibility in mixtures of immiscible polymers and improve the interfacial adhesion in composites and polymeric nanocomposites [29, 30].

Some studies have used MAH as a compatibilizing agent to increase the interactions between the polymer and fillers by introducing polar groups on the polymer backbones, as this can enhance the dispersion of the reinforcement [4, 23, 31, 32]. Ismail *et al*. [32] compared the behavior of EPDM and EPDM functionalized with MAH with different bentonite contents. All compatibilized samples showed increases in the vulcanization time (t_{90}) and scorch time (t_{S2}). Furthermore, the authors observed an increase in tensile strength in MAH-*g*-EPDM, which was attributed to the formation of hydrogen bonds between the EPDM and bentonite particles. Azizli *et al*. [23] investigated the compatibility of NR/EPDM-*g*-MAH/EPDM/GO nanocomposites with different GO contents. The addition of 1 and 3 phr GO increased t_{90} by approximately 6 and 8%, respectively. The tensile strength increased by approximately 28 and 64% with the addition of 1 and 3 phr GO, respectively, while the elongation increased by approximately 7 and 44%.

However, there are no reports of studies investigating the properties of EPDM nanocomposites functionalized with MAH and reinforced by GO or EBI-reduced GO. Therefore, the present study focuses on the use of GO nanoparticles reduced by EBI and the implementation of MAH as a compatibilizing agent between the nanoparticles and the elastomeric matrix. In this study, the effects of GO and rGO on the properties of nanocomposites based on EPDM and MAH-functionalized EPDM compounds were investigated. GO was synthesized using a modified Hummers method with a pre-oxidation step and was reduced by EBI. GO and rGO were characterized by Raman spectroscopy, X-ray diffraction (XRD), and scanning electron microscopy (SEM). The vulcanization characteristics, mechanical properties, hardness, and cross-linking density of the nanocomposites were analyzed.

2. Experimental

2.1. Materials

Graphite (Grafmax FP 120) with a carbon content of 99.98% was supplied by the National Graphite Company (Itapecerica, Brazil). The EPDM samples were provided by Exxon Mobil (Irving, USA) and had the trade names Vistalon® 6602 (55 wt% ethylene and 5.2% diene; Mooney viscosity (ML 1+4 (125°C) 80 MU) and Exxelor® VA 1803 (EPDM-*g*-MAH), *i.e*., MAH-functionalized EPDM (43 wt% ethylene and 4% diene) [33]. Exxelor® VA 1803 was used as a compatibilizer between the EPDM and GO or rGO; its melt index value was 3 g/10 min ±2 (ASTM D1238, 230 °C, 2.16 kg).

Chemical reagents such as sulfuric acid (98%, H_2SO_4), potassium persulfate ($K_2S_2O_8$), diphosphorus pentoxide (P_2O_5), sodium nitrate ($NaNO_3$), potassium permanganate (99%, $KMnO_4$), hydrogen peroxide (30%, H_2O_2), ethyl alcohol (C_2H_5OH), hydrochloric acid (10%, HCl), sodium borohydride ($NaBH_4$), THF, and toluene were obtained from Synth (Diadema, Brazil), CAAL (Araçatuba, Brazil), Sigma-Aldrich (Saint Louis, USA). These were used for GO and rGO synthesis and for their subsequent incorporation into EPDM.

2.2. Graphene oxide (GO) and reduced GO (rGO) preparation

Graphite (10 g) was pre-oxidized with sulfuric acid, potassium persulfate, and diphosphorus pentoxide. The dispersion was maintained at 80 °C for 6 h with continuous stirring. Subsequently, the dispersion was washed with distilled water and filtered to achieve a pH of approximately 7. Subsequently, the pre-oxidized material was dried in an oven at 60 °C for 24 h. This pre-oxidation step is essential to improve the oxidation level of the obtained material. In the next

step, pre-oxidized graphite was subjected to a modified Hummers method. The time and reagent concentrations were modified with reference to those reported in the literature [8] to improve the GO quality. Then, 460 ml of sulfuric acid and sodium nitrate (5.0 g) were added to the pre-oxidized graphite. The mixture was stirred continuously and maintained in an ice bath (temperature of approximately 5 °C) for 30 min. Subsequently, 30.0 g of potassium permanganate was added slowly over 30 min, and the reaction mixture was allowed to cool for another 30 min. Then, the dispersion was heated at 40 °C for 2 h. Next, 920 ml of deionized water was added, and the dispersion was stirred for 15 min. Hydrogen peroxide solution (50 ml) was added to the dispersion and stirred for 30 min. The dispersion gradually changed from dark greenish-black to yellow, indicating a high level of oxidation. The dispersion was then filtered using a Büchner funnel in a vacuum system with 1 l HCl. The material retained in the funnel was dialyzed against deionized water for 4 days until it reached a neutral pH. Subsequently, the material was subjected to ultrasonication for 1 h using a 19 mm probe and 70% amplitude, followed by centrifugation at 2000 rpm for 15 min. Centrifugation was applied to remove particles that were not completely oxidized.

GO dispersed in 50% ethanol and 50% water was irradiated by a JOB 188 Dynamitron (manufactured by Radiation Dynamics Inc., New York, USA) electron beam accelerator to obtain rGO. The dose rate was 2 kGy/s per cycle and the tray speed was 2 m/min. The total radiation dose was 80 kGy. The dispersion changed from brown to black after the electron beam reduction.

Finally, the resulting GO and rGO dispersions were lyophilized in a freeze dryer (FTS Systems (Stone Ridge, USA), Dura-Stop MP). The dispersions were maintained at –80 °C for 18–24 h. After that, the program applied was 20 min at –29 °C, followed by 120 min at –25° C, 120 min at –20 °C, 120 min at –15 °C, 120 min at –10 °C, 120 min at –5 °C, 200 min at 5 °C, 200 min at 15 °C, and 48 h at 20 °C. Throughout heat treatment, the system was maintained under a vacuum. Finally, the dried GO and rGO were individually ground in a SPEX (Metuchen, USA) 8000 high-energy mill for 5 min using tungsten carbide beads.

2.3. Nanocomposite preparation

For each composite, GO or rGO (0.5 g) was dispersed in THF (200 ml). The dispersion was subjected to ultrasonic tip treatment for 3 h using a 19 mm probe and 70% amplitude. Simultaneously, 5 g EPDM was dissolved in toluene (100 ml) at room temperature. Subsequently, the GO or rGO/THF dispersion was added to the EPDM solution, and the mixture was stirred for 15 h until GO or rGO was uniformly dispersed in the EPDM. Finally, the homogeneous dispersion was oven-dried at 60 °C, yielding a masterbatch of GO or rGO in EPDM. The same procedure was used to prepare a masterbatch with GO or rGO and MAH grafting in EPDM (EPDM-*g*-MAH). The steps for preparing the masterbatches are shown in Figure 1. The GO or rGO nanocomposites with and without MAH were prepared in two stages (Figure 2): i) the masterbatch was first mixed for 7 min in an internal mixer coupled to a Rheomix 600p torque rheometer (Haake (Waltham, USA), PolyLab900) at 140 °C and 50 rpm, totaling 70% of the chamber volume, and then ii) the nanocomposite formulations were processed by two-roll mill mixing (Mecanoplast (Rio Claro, Brazil), model C400). Each vulcanizing agent used in the formulation was added separately and mixed for 5 min at a controlled temperature of 60 °C. The different compositions are presented in Table 1 in parts per hundred rubber [phr]. Zinc oxide, stearic acid, sulfur, and *N*-cyclohexyl-2-benzothiazole sulfenamide (CBS) were used as vulcanization agents [34, 35]. Oil-styrenated phenol (Protetox NS®) was used as an antioxidant. For comparison, EPDM and EPDM-*g*-MAH without fillers were also dissolved in toluene and prepared via the same procedures described for the nanocomposites.

2.4. Characterization techniques

Pristine graphite, GO, and rGO were characterized by spectroscopy using a WITEC Raman microscope (Alpha 300 R). The vibrations of the molecules were excited using a 532 nm laser. XRD measurements were also performed to characterize the structures of pristine graphite, GO, and rGO using a Rigaku powder diffractometer (Miniflex) with copper as the X-ray source (1.5418 Å), steps of 0.02°, and a soaking time of 5 s. The *d*-spacings of the pristine graphite, GO, and rGO were calculated using Bragg's equation [36]. At least three measurements using both techniques were obtained from each sample.

The morphologies, atomic compositions, and morphologies of the pristine graphite, GO, and rGO were examined using an FEI Inspect F50 SEM. The morphologies of the EPDM compounds (EPDM and

EPDM-*g*-MAH) and nanocomposites (GO/EPDM, GO/EPDM-*g*-MAH, rGO/EPDM, and rGO/EPDM-*g*-MAH) were observed by field-emission SEM (FE-SEM, TESCAN, MIRA3). Energy-dispersive spectroscopy (EDS) was used to analyze the chemical composition of the GO or rGO nanoparticles. The GO and rGO materials were sputter-coated with gold and the nanocomposites with platinum.

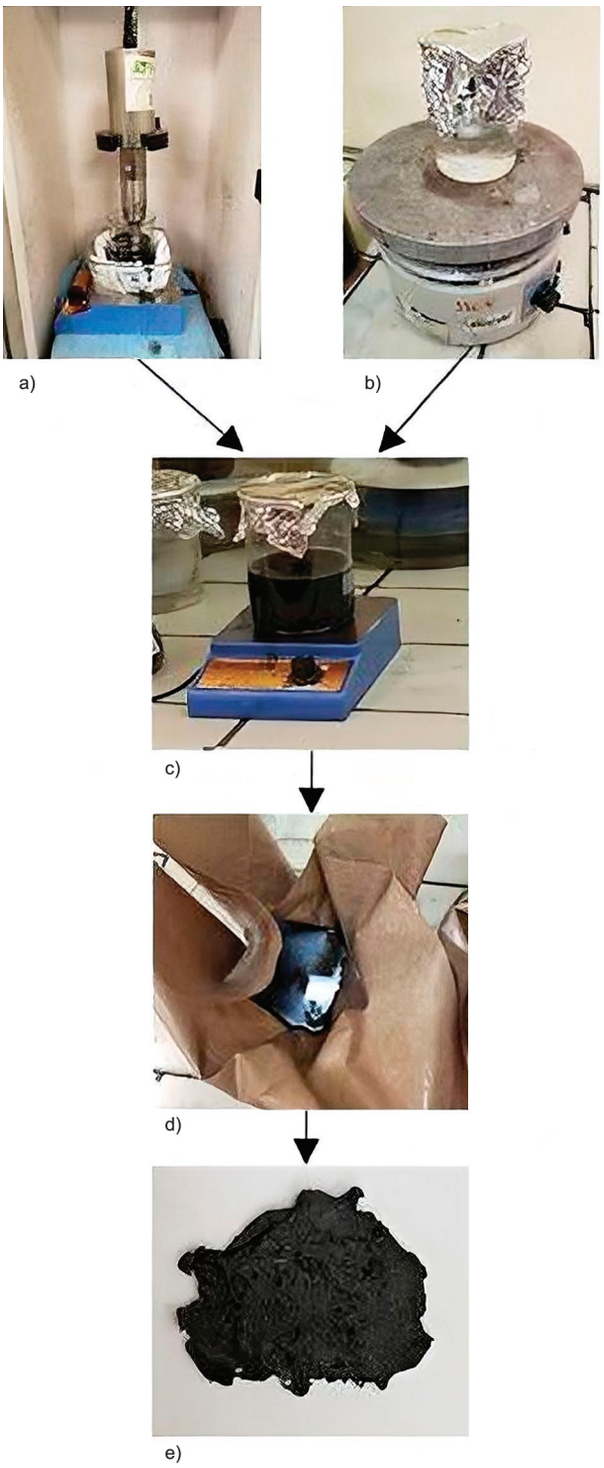

Figure 1. Masterbatch preparation process: (a) ultrasonic tip treatment of GO or rGO in THF, (b) homogenization of EPDM or EPDM-*g*-MAH in toluene, (c) mixture of GO or rGO and EPDM or EPDM-*g*-MAH in THF and toluene, (d) drying at room temperature, (e) masterbatch after drying.

The cure vulcanization properties of the EPDM or EPDM-*g*-MAH compounds and the nanocomposites were measured at 170 °C using an oscillating disc rheometer (ODR 2000 TEAM), based on ASTM D2084 [37]. The cure properties were obtained, including the scorch time (t_{S2}), optimal cure time (t_{90}), cure rate index ($CRI = 100/(t_{90} - t_{S2})$), maximum torque ($M_H$), minimum torque ($M_L$), and the difference between the maximum and minimum torques ($\Delta M = M_H - M_L$).

The crosslink densities of the EPDM or EPDM-*g*-MAH compounds and nanocomposites were determined based on rapid solvent-swelling measurements (decalin for 72 h at room temperature) by applying the Flory–Rehner equation [35, 38–40] as Equation (1):

$$\nu = \frac{1}{2M_c} \tag{1}$$

where M_c is defined in Equation (2):

$$M_c = -\frac{\rho_p \nu_n V_{rf}^{1/3}}{\ln(1 - V_r) + V_{rf} + \chi V_{rf}^2} \tag{2}$$

where M_c, ρ_p, and ν_n are the molecular weight of crosslinking, EPDM density, and molar volume of the solvent, respectively. V_{rf} is the volume fraction of the EPDM in the swollen mass (Equation (2)). χ is the coefficient of interaction between the rubber network and solvent and is calculated according to Equation (3) and (4):

$$\chi = \beta + \frac{\nu_n}{RT}(\delta_s - \delta_p)^2 \tag{3}$$

$$V_{rf} = \frac{(d - fw)\rho_p^{-1}}{(d - fw)\rho_p^{-1} + A_s \rho_s^{-1}} \tag{4}$$

where δ_s and δ_p are the solubility parameters of the solvent (8.8 cal/cm$^{1/2}$) and rubber (8.1 cal/cm$^{1/2}$) network [41], respectively. R is the universal gas constant (8.314 J/(mol·K)), T is the absolute temperature, and β is the lattice constant. V_{rf} was calculated using Equation (4). The V_{rf} calculation considered only the fraction of rubber compounds and discounted the filler content using the empirical density for each reinforcement [42], where d is the de-swollen weight of the sample, f is the volume fraction of the

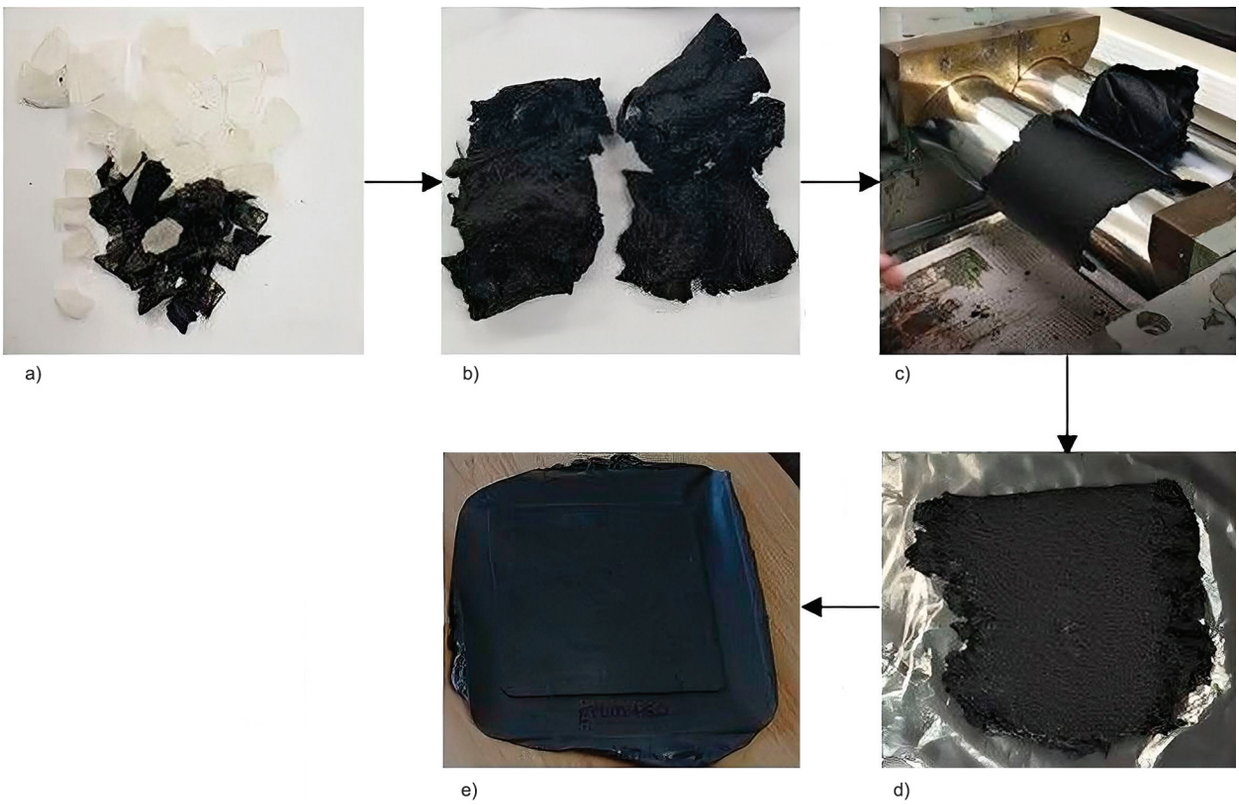

Figure 2. Processing of GO or rGO/EPDM or EPDM-*g*-MAH nanocomposites: (a) dried masterbatch of GO or rGO, and pieces of EPDM or EPDM-*g*-MAH, (b) EPDM or EPDM-*g*-MAH + GO or rGO masterbatch before and after processing in torque rheometer, (c) mixing the nanocomposite in a two-roll mill with vulcanizing agents, (d) the nanocomposite before pressing, and (e) the nanocomposite after pressing.

Table 1. Formulation of EPDM and EPDM-*g*-MAH rubber compounds and nanocomposites in parts per hundred rubber (phr).

	EPDM	EPDM-*g*-MAH	GO or rGO/EPDM	GO or rGO/EPDM-*g*-MAH
EPDM	100	96.87	100	96.87
EPDM-g-MAH	0	3.13	0	3.13
GO or rGO	0	0	1.25	1.25
ZnO (zinc oxide)	5	5	5	5
Stearic acid	2	2	2	2
Antioxidant oil	2	2	2	2
Sulfur (S_8)	2	2	2	2
CBS	1	1	1	1

fiber, w is the initial weight of the sample, ρ_s is the density of the solvent, and A_s is the amount of solvent absorbed by the sample. The crosslinking density (v) was equivalent to $1/(2M_c)$ (Equation (1)).

The tensile strength measurements of the composites and nanocomposites were conducted based on ASTM D412 [43] using a Kratos KE-3000 universal testing machine with a load cell of 1 kN and a crosshead speed of 500 mm/min.

The rubber hardness was determined using a Bareiss hardness tester (model HP) based on ASTM D1415 [44]. The reported results are the average of measurements taken at five different points on each specimen.

3. Results and discussion

3.1. GO and rGO characterization

Figure 3 and Table 2 show the Raman spectra and peak values for the pristine graphite, GO, and rGO. The pristine graphite spectrum displayed a prominent G peak at 1593 cm^{-1}; this was attributed to the C=C stretching modes of the graphitic structures (sp^2 domains). The positions and full widths at half maximum (FWHM) of the D, G, and 2D bands were determined. The FWHM of the G peak was 22.8 cm^{-1}, which indicated that the peak originated from the stretching vibrations of the carbon bonds in the rings of the sp^2-hybridized graphene layers. The FWHM

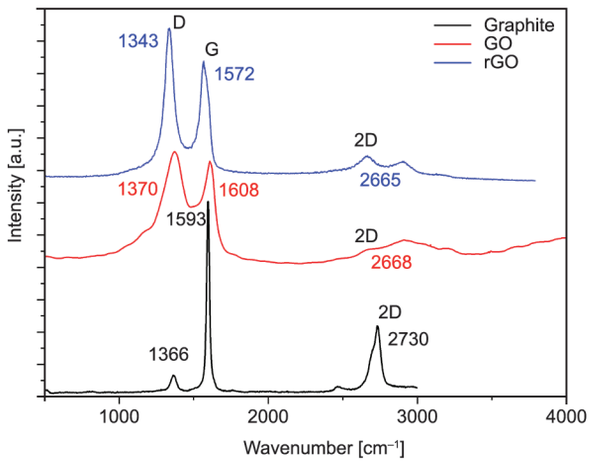

Figure 3. Raman spectra of graphite, GO, and rGO.

Table 2. Full width at half maximum (FWHM) values and position of the bands in the Raman spectra of graphite, GO, and rGO.

Samples	D band/FWHM [cm^{-1}]	G band/FWHM [cm^{-1}]	2D band [cm^{-1}]	I_D/I_G [–]
Graphite	1366/49.9	1593/22.8	2730	0.18
GO	1370/207.6	1608/170.1	2668	1.05
rGO	1343/75.1	1572/71.8	2665	1.23

of the D band was 49.9 cm^{-1}. This large FWHM indicated that the structure was perturbed, for example, by the presence of heteroatoms or point dislocations in the structure; this band is not observed in the Raman spectrum of perfect graphite. However, the structure of graphite was still well-ordered, as confirmed by the I_D/I_G ratio of 0.18, which indicated relatively few defects in the graphite structure.

The spectrum of GO showed broadening in the G and D bands, indicating the presence of vacancies or dislocations in the graphitic structure owing to the change of certain sp^2 bonds to sp^3 as a result of the oxygen attachment, representative of a successful oxidation process. The I_D/I_G ratio for GO was 1.05, indicating a higher density of defects induced by the oxidation process. The 2D band was less intense than the D band. For graphene monolayers, the 2D band appears as a single peak near 2675 cm^{-1}. In contrast, the 2D band of the two graphene layers comprised four peaks: D*, 2D, D+D, and 2D.

The Raman spectrum of rGO showed an even higher ID/IG ratio than those of GO and pristine graphite, indicating the formation of new defects in the structures during the reduction process. The FWHM values of the D and G bands were lower than those of GO; this difference is associated with the lower content of oxygen groups in rGO and the regeneration of the graphite structure.

Figure 4 and Table 3 present the XRD patterns of graphite, GO, and rGO and their corresponding peak characterization values.

Table 3. Comparison of structural parameters of graphite, GO, and rGO derived from XRD patterns.

		Graphite	GO	rGO
2θ	[°]	26.3	10.1	22.25/11.08
d	[nm]	0.34	0.87	0.40/0.79
hkl[a]		002	001	002/001

[a]*h*, *k*, and *l* are Miller indices.

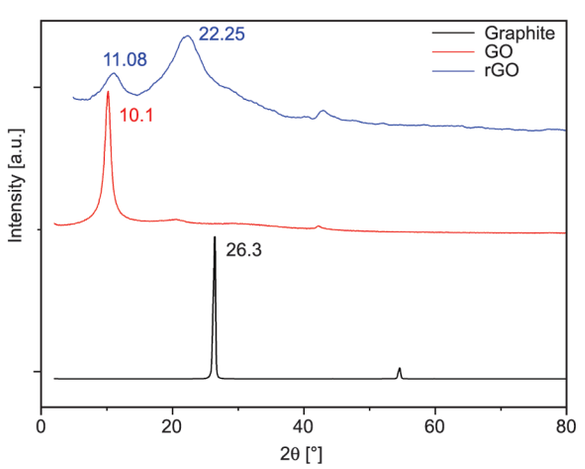

Figure 4. XRD patterns of graphite, GO, and rGO.

XRD was used to determine the crystal structure and lattice parameters of the samples. During the oxidation process, it was observed that the intense peak of the (002) plane (*d*-spacing = 3.4 Å, 2θ = 26.3°) of the graphite flakes gradually decreased and vanished, while the peak corresponding to the (001) plane (10.1°) appeared and increased, indicating an increase in interplanar distance from 3.4 to 8.7 Å, what was caused by the presence of oxygen functional groups between the GO sheets. As GO was reduced to rGO, the ordered crystal structure was partially restored. This was verified by the appearance of the (002) diffraction peak at 22.25°. It is clearly observed that an (001) diffraction peak remained at 11.08° with a lower intensity, indicating that GO was not fully reduced. This result is desirable for achieving better rGO dispersion in the elastomer, facilitated by the remaining oxygen-containing functional groups in the graphene sheets.

Figure 5 shows the morphologies of GO and rGO, and the EDS spectra.

As shown, GO featured wrinkled and kinked areas (Figure 5a), owing to the oxygen-containing functional

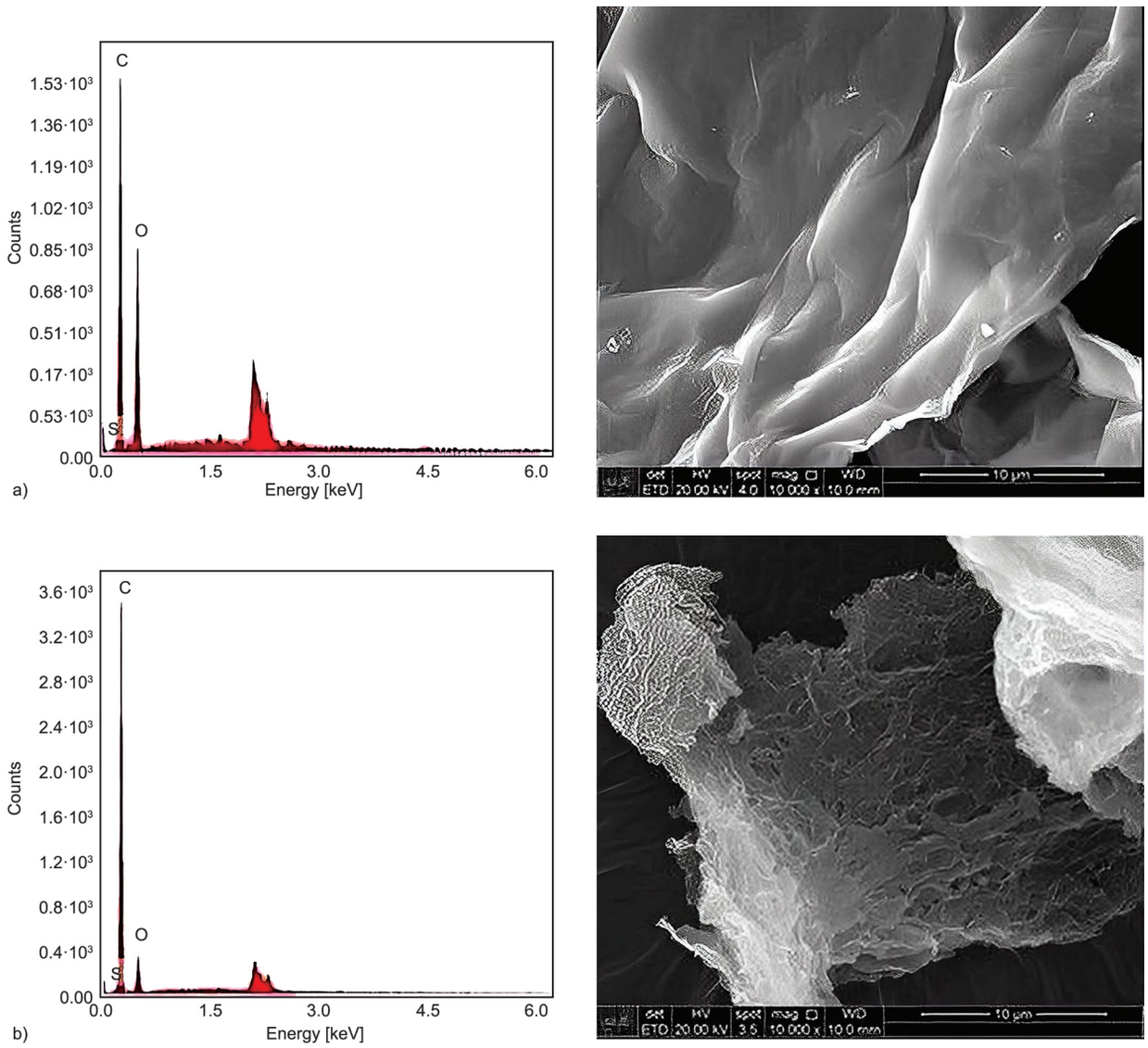

Figure 5. EDS spectra and SEM images of (a) GO and (b) rGO at 10 000× magnification.

groups that changed some of the carbon hybridizations from sp^2 to sp^3. Individual sheets can be clearly differentiated on the basis of their edges. They were intercalated with rough surfaces, resulting from structural deformation upon exfoliation. In contrast, rGO exhibited thin, wrinkled sheets and fluffy structures (Figure 5b). The EDS spectra are shown in Figures 5a and 5b. The rGO C/O ratio (5.4) was 3.5 times higher than that of GO (1.6), demonstrating a lower oxygen content.

3.2. Morphological characterization of the compounds and nanocomposites

Figure 6 shows surface SEM images of the EPDM and EPDM-*g*-MAH compounds and nanocomposites containing GO and rGO.

Figure 6 shows the continuous structure of EPDM compounds; in these images, GO and rGO sheets could not be distinguished on the surfaces, indicating that the method for nanofiller incorporation was effective for reinforcement dispersion. Some whitish agglomerates were evident in Figures 6a–6d, as indicated by red circles. To identify these structures, EDS analysis was performed on the EPDM compound without MAH in the agglomerated regions; the results showed evidence of zinc, introduced as ZnO, a vulcanizing agent, in these structures (Figure 7).

The addition of the MAH compatibilizer to the formulations clearly improved the dispersion of vulcanizing agents such as zinc oxide. In addition, the surfaces of formulations containing MAH had a slightly wrinkled texture.

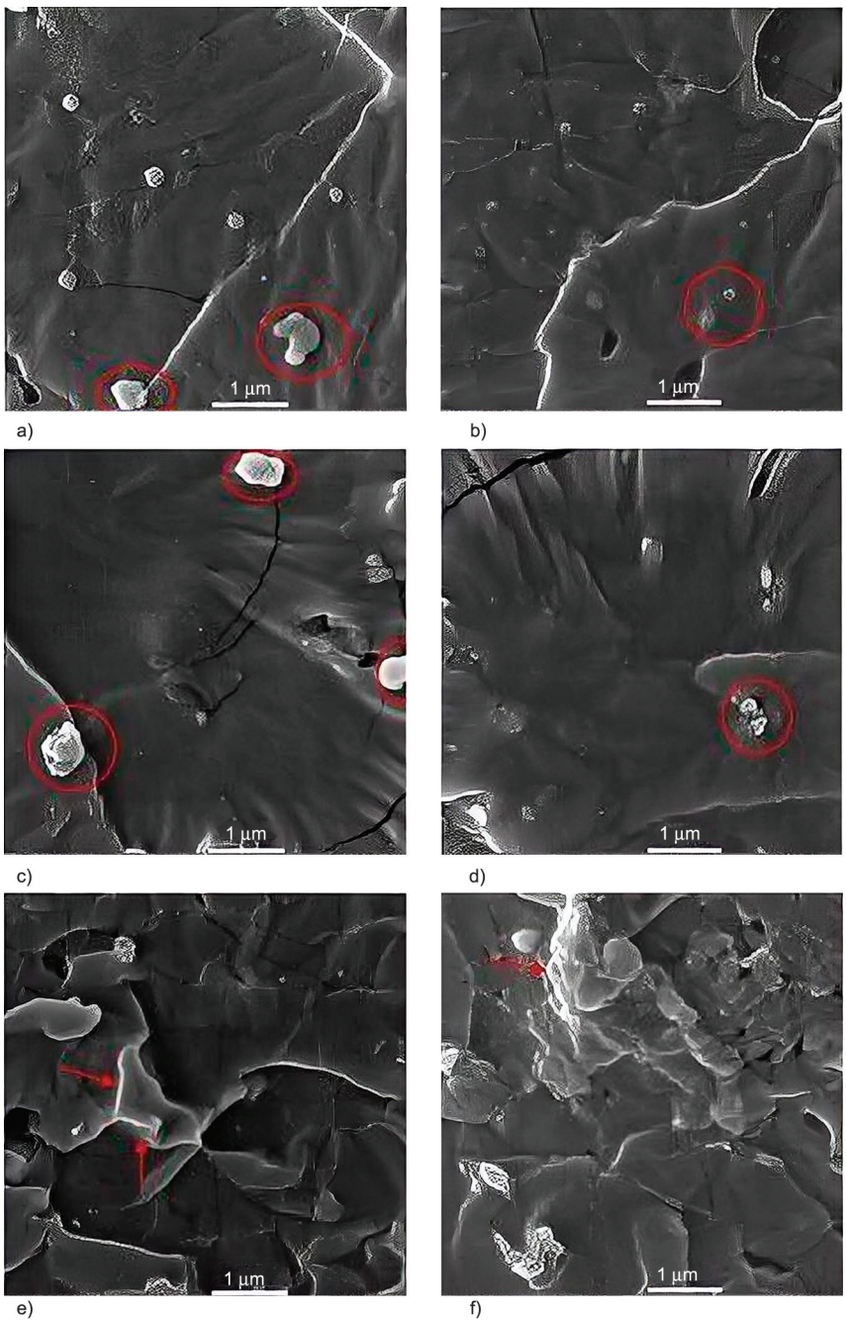

Figure 6. SEM images of (a) EPDM compound, (b) EPDM-*g*-MAH compound, (c) GO/EPDM, (d) GO/EPDM-*g*-MAH, (e) rGO/EPDM, and (f) rGO/EPDM-*g*-MAH at 50 000× magnification.

Some whitish spots were indicated by red arrows in the contours of the wrinkled surfaces and in the fractured regions for the rGO nanocomposites with and without the MAH compatibilizer (Figure 6e and 6f). Mensah *et al*. [19] observed similar features in micrographs and attributed the spots on the surfaces of these nanocomposites to the presence of ZnO particles.

3.3. Vulcanization behavior of the compounds and nanocomposites

The vulcanization curves of the EPDM compounds and nanocomposites with GO and rGO are shown in Figure 8. All the parameters obtained from the vulcanization curves are presented in Table 4.

Table 4 presents the values of M_L, M_H, ΔM, scorch time (t_{S2}), optimal vulcanization time (t_{90}), and *CRI*

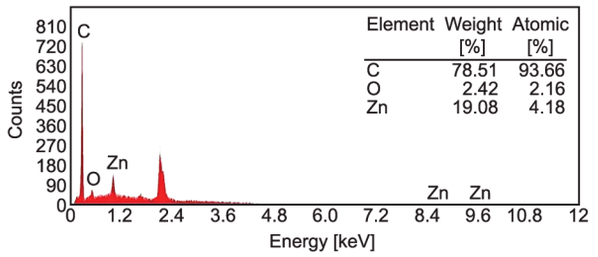

Figure 7. Semi-quantitative elemental analysis by EDS of EPDM compound.

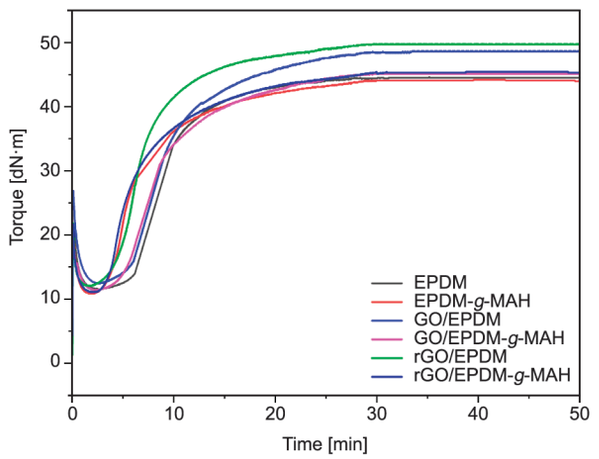

Figure 8. Rheometric curves for EPDM compounds and GO and rGO nanocomposites.

obtained from the EPDM compounds and nanocomposites containing GO and rGO, with and without MAH. The results of crosslinking density measurements are listed in Table 4.

The introduction of GO and rGO to the EPDM directly influences the vulcanization process. As shown in Table 4, the addition of GO increased the optimal vulcanization time and reduced the CRI of the EPDM compounds. However, the addition of rGO did not result in the same behavior. It is suggested that the greater number of oxide groups present on the surface of GO delays the vulcanization reactions [19, 20]. In our study, a decrease in t_{S2} was observed in the GO and rGO nanocomposites without the compatibilizer. Azizli *et al*. [23] reported similar results and hypothesized that the degree of unsaturation of the EPDM rubber could influence the initial induction reactions between GO and vulcanizing agents. Coran [45] proposed that curing reactions in formulations using vulcanization accelerators, such as the CBS sulfonamide used in this work, occur in several steps and via different routes. The accelerator reacts with sulfur to produce monomeric polysulfides, which react with rubber to form polysulfides. Polysulfides react either directly or through intermediate compounds to form crosslinks. In EPDM, before the formation of crosslinks, the rubber is first sulfurated by accelerator-derived polysulfides to yield macromolecular polysulfidic intermediates [45, 46]. The GO and rGO nanoparticles participate in these reactions with sulfur, zinc oxide, stearic acid, and CBS affecting the rate of each partial reaction according to the content of each component [46]. The reactions that occurred initially had a higher speed than the final-sequence reactions [20], which explains the decrease in t_{S2} and increase in the optimal vulcanization time. Mensah *et al*. [19] reported that during vulcanization, sulfur reactions in EPDM compounds occur at the double bonds of ethylidene norbornene (ENB) sites. However, these reactions do not occur at ENB unsaturation but rather activate the allylic positions, resulting in isomerism to produce sulfide species, as illustrated in Figure 9a. When introduced as reinforcements, GO and rGO reacted with the vulcanization agents, forming an additional crosslinked structure with the EPDM. Wu *et al*. [20] reported that the addition of oxygenated groups, such as the hydroxyl and carboxyl groups of GO and rGO, induced reactions with vulcanization accelerators to generate polysulfide species that formed crosslink precursors, resulting in polysulfidic crosslinks (Figure 9b). An

Table 4. Characteristic parameters of vulcanization curves of the EPDM compounds and the GO and rGO nanocomposites, with or without MAH.

Sample	t_{90} [min]	t_{S2} [min]	M_H [dN·m]	M_L [dN·m]	ΔM^a [dN·m]	CRI^b [min]	Crosslinking density ·10^{-5} [g·mol/cm^3]
EPDM	15.49	6.06	44.5	11.5	33.0	10.6	4.16
EPDM-*g*-MAH	16.25	3.50	44.1	10.9	33.2	7.8	3.78
GO/EPDM	18.29	5.41	48.6	12.4	36.2	7.8	4.24
GO/EPDM-*g*-MAH	18.15	4.85	45.2	11.4	33.8	7.6	4.02
rGO/EPDM	14.74	3.68	49.8	12.0	37.9	9.0	4.33
rGO/EPDM-*g*-MAH	16.91	3.47	45.4	11.1	34.4	7.4	4.17

[a]$\Delta M = M_H - M_L$

[b]$CRI = 100/(t_{90} - t_{S2})$, cure rate index.

increase in the maximum torque of the GO and rGO nanocomposites compared to that of the EPDM was also observed and was attributed to the restriction of the chain movement with the addition of reinforcement.

The EPDM-*g*-MAH and rGO/EPDM-*g*-MAH nanocomposites exhibited an increase in the optimal vulcanization time compared with the unfunctionalized EPDM compounds and rGO/EPDM nanocomposites. This can be attributed to the acid and anhydride groups involved in the vulcanization reactions [30], or possibly to the lower diene content in the composition of EPDM-*g*-MAH. Shanmugharaj *et al*. [21] demonstrated that certain acid groups can absorb the basic species of accelerators, thus delaying the vulcanization of natural rubber. Coran [47] also found that the effects of acids and anhydrides can delay vulcanization reactions, with the effects of EPDM-*g*-MAH being greater than those of unmodified EPDM. Stiehler and Wakelin [48] proved that an acidic pH slows vulcanization reactions. The authors mentioned that if all components are soluble, the pH of the system governs the proportion of acid that combines with zinc. In contrast, the GO-functionalized nanocomposites (GO/EPDM-*g*-MAH) did not show significant differences in optimal vulcanization time relative to the unfunctionalized nanocomposites. Therefore, the simultaneous addition of MAH and GO did not synergistically influence vulcanization properties. This can be attributed to the excessive increase in oxygen-containing functional groups from the GO sheets and MAH during the vulcanization step. Moreover, M_H, M_L, and ΔM decreased for all functionalized samples, suggesting that MAH also acted as a plasticizer in the formulation.

It is possible that the lower content of diene in the composition of EPDM-*g*-MAH compared to that in the EPDM resin also reduced the crosslinking density of EPDM-*g*-MAH and GO or rGO/EPDM-*g*-MAH nanocomposites. In the curing reaction, MAH reacts with the diene structures and occupies sites for potential crosslinking, thereby suppressing the interactions between GO or rGO and EPDM [23]. Considering that vulcanization reactions occur via different routes and mechanisms, it is supposed that crosslinking is favorably generated from the reactions between the vulcanization agents and the oxygen-containing functional groups of MAH and GO or rGO (Figure 9c).

The GO and rGO/EPDM nanocomposites exhibited a small increase in crosslinking density compared to the EPDM compound. The hydroxyl groups present in GO and rGO are electron donors in vulcanization reactions, increasing the nanofiller–EPDM interactions, thereby contributing to increased crosslinking. Thus, the solvent permeation in the nanocomposites decreased compared to that in the EPDM compound [49].

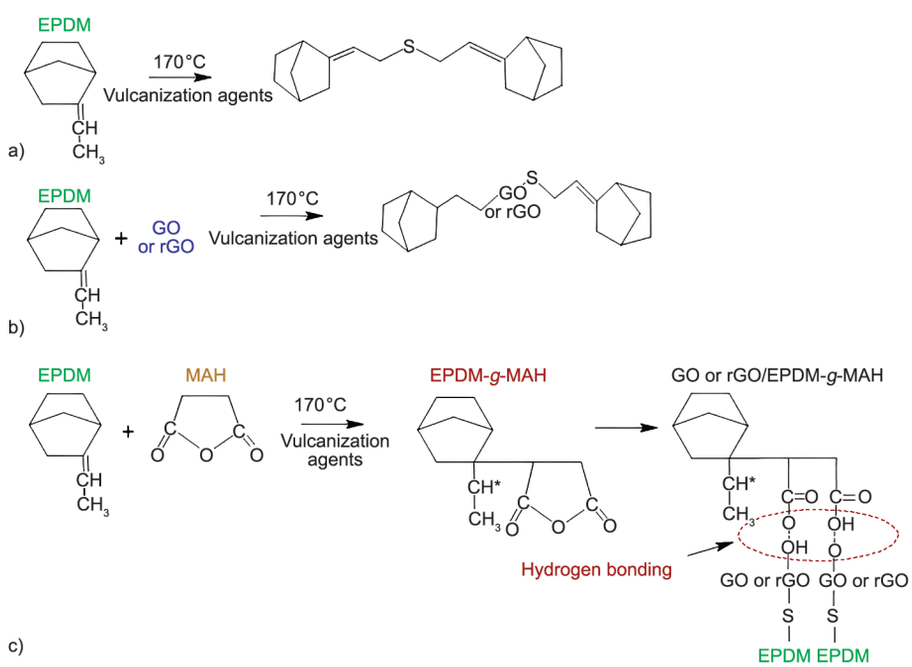

Figure 9. General scheme for the possible structures formed from (a) the vulcanization of EPDM, (b) EPDM nanocomposites with GO or rGO, (c) GO or rGO/EPDM-*g*-MAH nanocomposites [20, 23, 50].

3.4. Mechanical properties of the compounds and nanocomposites

Figure 10 and Table 5 present the results obtained from the tensile tests performed on the EPDM compounds and nanocomposites containing GO and rGO. The addition of MAH to the EPDM compounds and GO and rGO nanocomposites increased their tensile strengths and elongations. The tensile strength of the EPDM-*g*-MAH compounds were increased by approximately 10% compared to that of the EPDM compound. When comparing the GO and rGO/EPDM-*g*-MAH nanocomposites with the GO and rGO/EPDM nanocomposites, the tensile strength increased by approximately 5 and 20%, respectively. Furthermore, a higher increase in the elongation values of the rGO-containing nanocomposites was observed relative to

Table 5. Mechanical properties and Shore A hardness of EPDM compounds and nanocomposites with GO and rGO.

	Tensile strength [MPa]	Tensile modulus at 100% elongation [MPa]	Elongation at break [%]	Hardness [Shore A]
EPDM	1.40±0.09	1.38±0.02	99±16	50.6±0.5
EPDM-*g*-MAH	1.54±0.07	1.34±0.03	126±7	49.6±0.5
GO/EPDM	1.92±0.11	1.57±0.08	141±9	52.3±0.5
GO/EPDM-*g*-MAH	2.02±0.17	1.45±0.03	166±19	51.4±0.3
rGO/EPDM	2.22±0.12	1.52±0.02	175±13	52.9±0.3
rGO/EPDM-*g*-MAH	2.66±0.15	1.63±0.04	195±17	52.6±0.5

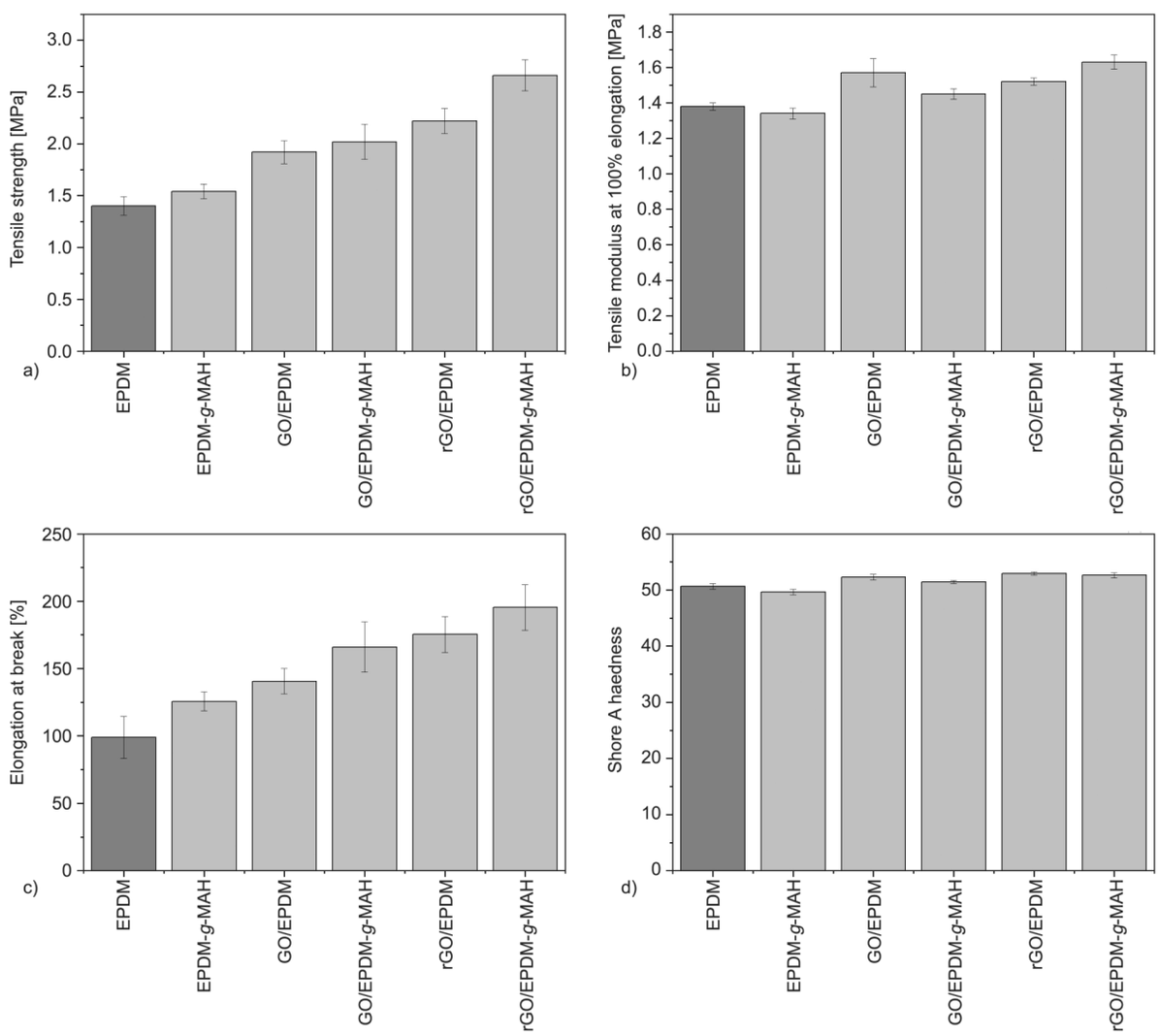

Figure 10. Tensile test results of EPDM compounds and nanocomposites with GO and rGO: (a) tensile strength, (b) tensile modulus at 100% elongation, (c) elongation at break, and (d) Shore A hardness.

those of the GO-containing composites. Besides, the introduction of MAH increased the elongation by 18% for the nanocomposites with GO and 11% for the nanocomposites with rGO compared to the elongations measured from unfunctionalized nanocomposites.

The MAH-functionalized EPDM resulted in stronger intermolecular interactions, which improved the mechanical properties of the compound. As discussed in Section 3.3, it is likely that MAH chemically reacts with the oxygen-containing functional groups attached to graphene sheets. This reaction provided nanocomposites with better dispersion in the EPDM matrix. The increase in maximum stress is also attributed to reactions with the hydroxyl functional groups of GO with the EPDM-*g*-MAH structure, owing to the formation of hydrogen bonds between GO and rGO with the oxide groups of EPDM-*g*-MAH (Figure 9) [23].

These results are similar to those reported by Ismail *et al*. [32] and Pasbakhsh *et al*. [50]. These authors evaluated the influence of EPDM with MAH as a compatibilizer and other nanoparticles, such as bentonite and halloysite, and found that MAH contributed to improvements in the mechanical properties of the nanocomposites, especially in tensile strength. The enhancement in the mechanical properties was attributed to the MAH-promoted compatibility between the nanofillers and EPDM.

The differences between the unfunctionalized GO and rGO nanocomposites and the unfunctionalized EPDM compound were remarkable, mainly in terms of the tensile strength and elongation at break. The GO nanocomposites exhibited increases in tensile strength and elongation, of 37 and 42%, respectively; nanocomposites with rGO exhibited increases of 59 and 77%, respectively. Although both types of nanoparticles contributed to the improvement in the mechanical properties, better performance was observed for the formulations containing rGO. These results can be attributed to (i) the partial recovery of the sp^2 graphite structure in the graphene sheets of rGO and (ii) the higher similarity in polarity between rGO and the EPDM elastomer. Mensah *et al*. [19] obtained similar results, that is, the mechanical properties of nanocomposites with rGO overlapped with those of GO.

The EPDM-*g*-MAH compound and nanocomposites (GO or rGO/EPDM-*g*-MAH) did not show significant differences in modulus values at 100% elongation. However, unfunctionalized GO or rGO nanocomposite formulations showed values more than 10% higher than those of the unfunctionalized EPDM compound. The increase in the modulus is related to the restriction of chain mobility caused by the addition of reinforcements.

The Shore A hardness of the unfunctionalized EPDM compound was 50.6, as reported in the literature [51, 52]. The hardness of the MAH-functionalized EPDM compound was reduced by only 2%. In contrast, the addition of GO and rGO increased the hardness of the unfunctionalized EPDM nanocomposites by up to 4.5%. Similar results were reported by Azizli *et al*. [23]. No significant change in hardness was observed with the inclusion of MAH in the nanocomposites containing GO or rGO.

4. Conclusions

The effects of GO and rGO on the properties of EPDM compounds and MAH-functionalized EPDM compounds were investigated. Based on the results obtained in this study, it is possible to conclude, from the rheological characteristics, that (i) the EPDM-*g*-MAH compound and nanocomposites showed a reduction in the crosslinking density compared to unfunctionalized EPDM compounds and nanocomposites; (ii) the curing reactions were slower for the nanocomposites produced with GO, possibly owing to the greater amount of oxygenated groups on the surfaces of the sheets of the nanoparticles, compared to those for rGO; and (iii) when GO and rGO were introduced into EPDM compounds, an increase in the maximum torque was observed, which could be attributed to the restriction of chain movement caused by the reinforcements. In addition, (iv) the MAH-functionalized EPDM compound and GO/EPDM-*g*-MAH nanocomposites had longer curing times, possibly owing to the presence of acid and anhydride groups, which delayed the vulcanization reactions.

From the analyses of the mechanical properties, it was possible to conclude that: (i) EPDM compounds and GO or rGO nanocomposites functionalized with MAH showed higher tensile strength and elongation than the unfunctionalized compounds and composites; (ii) MAH contributed to the greater dispersion of GO or rGO in the nanocomposites, and (iii) the nanocomposites with rGO nanoparticles showed improved mechanical performance.

Finally, despite the good physicochemical affinity between MAH and GO, their simultaneous addition

to the EPDM compounds did not synergistically improve the vulcanization and mechanical properties because of the excessive number of oxygen-containing functional groups present during the vulcanization process.

Acknowledements

The authors would like to thank CAPES (Coordination for the Improvement of Higher Education Personnel) for financial support from the PNPD project nº 88887.373623/2019-00 – Brazil, Proex number 0727/2020; the Laboratory of Microelectronics (LME) of the Department of Electronic Systems Engineering, Polytechnic School, USP; Dr. Marcio Yee (Marine Science Department, Federal University of São Paulo-UNIFESP); Dr. Antonio José Piantino Ferreira and Dr. Claudete Serrano Astolfi Ferreira from the School of Veterinary Medicine and Animal Science, USP; and Dr. Evaldo José Corat from the National Institute for Space Research (INPE).

References

[1] Kim H., Abdala A. A., Macosko C. W.: Graphene/polymer nanocomposites. Macromolecules, **43**, 6515–6530 (2010).
https://doi.org/10.1021/ma100572e

[2] Papageorgiou D. G., Kinloch I. A., Young R. J.: Graphene/elastomer nanocomposites. Carbon, **95**, 460–484 (2015).
https://doi.org/10.1016/j.carbon.2015.08.055

[3] Chen B., Ma N., Bai X., Zhang H., Zhang Y.: Effects of graphene oxide on surface energy, mechanical, damping and thermal properties of ethylene-propylene-diene rubber/petroleum resin blends. RSC Advances, **2**, 4683–4689 (2012).
https://doi.org/10.1039/C2RA01212J

[4] Surya I., Muniyadi M., Ismail H.: A review on clay-reinforced ethylene propylene diene terpolymer composites. Polymer Composites, **42**, 1698–1711 (2021).
https://doi.org/10.1002/pc.25956

[5] Alkhouzaam A., Qiblawey H., Khraisheh M., Atieh M., Al-Ghouti M.: Synthesis of graphene oxides particle of high oxidation degree using a modified Hummers method. Ceramics International, **46**, 23997–24007 (2020).
https://doi.org/10.1016/j.ceramint.2020.06.177

[6] Azizli M. J., Barghamadi M., Rezaeeparto K., Mokhtary M., Parham S., Goodarzi V., Soltani S.: Enhancement of thermal, morphological, and mechanical properties of compatibilized based on PA6-enriched graphene oxide/EPDM-*g*-MA/CR: Graphene oxide and EPDM-*g*-MA compatibilizer role. Journal of Applied Polymer Science, **138**, 49901 (2021).
https://doi.org/10.1002/app.49901

[7] Brodie B. C.: On the atomic weight of graphite. Philosophical Transactions, **149**, 249–259 (1859).
https://doi.org/10.1098/rstl.1859.0013

[8] Hummers W. S., Offeman R. E.: Preparation of graphitic oxide. Journal of the American Chemical Society, **80**, 1339 (1958).
https://doi.org/10.1021/ja01539a017

[9] Botas C., Álvarez P., Blanco P., Granda M., Blanco C., Santamaría R., Romasanta L. J., Verdejo R., López-Manchado M. A., Menéndez R.: Graphene materials with different structures prepared from the same graphite by the Hummers and Brodie methods. Carbon, **65**, 156–164 (2013).
https://doi.org/10.1016/j.carbon.2013.08.009

[10] Paredes J. I., Villar-Rodil S., Martínez-Alonso A., Tascón J. M. D.: Graphene oxide dispersions in organic solvents. Langmuir, **24**, 10560–10564 (2008).
https://doi.org/10.1021/la801744a

[11] Konios D., Stylianakis M. M., Stratakis E., Kymakis E.: Dispersion behaviour of graphene oxide and reduced graphene oxide. Journal of Colloid and Interface Science, **430**, 108–112 (2014).
https://doi.org/10.1016/j.jcis.2014.05.033

[12] Wu R., Wang Y., Chen L., Huang L., Chen Y.: Control of the oxidation level of graphene oxide for high efficiency polymer solar cells. RSC Advances, **5**, 49182–49187 (2015).
https://doi.org/10.1039/C5RA02099A

[13] Sengupta I., Chakraborty S., Talukdar M., Pal S. K., Chakraborty S.: Thermal reduction of graphene oxide: How temperature influences purity. Journal of Materials Research, **33**, 4113–4122 (2018).
https://doi.org/10.1557/jmr.2018.338

[14] Agarwal V., Zetterlund P. B.: Strategies for reduction of graphene oxide – A comprehensive review. Chemical Engineering Journal, **405**, 127018 (2021).
https://doi.org/10.1016/j.cej.2020.127018

[15] Olorunkosebi A. A., Eleruja M. A., Adedeji A. V., Olofinjana B., Fasakin O., Omotoso E., Oyedotun K. O., Ajayi E. O. B., Manyala N.: Optimization of graphene oxide through various Hummers' methods and comparative reduction using green approach. Diamond and Related Materials, **117**, 108456 (2021).
https://doi.org/10.1016/j.diamond.2021.108456

[16] Botas C., Álvarez P., Blanco C., Santamaría R., Granda M., Gutiérrez M. D., Rodríguez-Reinoso F., Menéndez R.: Critical temperatures in the synthesis of graphene-like materials by thermal exfoliation-reduction of graphite oxide. Carbon, **52**, 476–485 (2013).
https://doi.org/10.1016/j.carbon.2012.09.059

[17] Yang Y., Chen L., Li D-Y., Yi R-B., Mo J-W., Wu M-H., Xu G.: Controllable reduction of graphene oxide by electron-beam irradiation. RSC Advances, **9**, 3597–3604 (2019).
https://doi.org/10.1039/C8RA06797J

[18] Jung J-M., Jung C-H., Oh M-S., Hwang I-T., Jung C-H., Shin K., Hwang J., Park S-H., Choi J-H.: Rapid, facile, and eco-friendly reduction of graphene oxide by electron beam irradiation in an alcohol-water solution. Materials Letters, **126**, 151–153 (2014).
https://doi.org/10.1016/j.matlet.2014.04.059

[19] Mensah B., Kang S. I., Wang W., Nah C.: Effect of graphene on polar and nonpolar rubber matrices. Mechanics of Advanced Materials and Modern Processes, **4**, 1 (2018).
https://doi.org/10.1186/s40759-017-0034-0

[20] Wu J., Xing W., Huang G., Li H., Tang M., Wu S., Liu Y.: Vulcanization kinetics of graphene/natural rubber nanocomposites. Polymer, **54**, 3314–3323 (2013).
https://doi.org/10.1016/j.polymer.2013.04.044

[21] Shanmugharaj A. M., Bae J. H., Lee K. Y., Noh W. H., Lee S. H., Ryu S. H.: Physical and chemical characteristics of multiwalled carbon nanotubes functionalized with aminosilane and its influence on the properties of natural rubber composites. Composites Science and Technology, **67**, 1813–1822 (2007).
https://doi.org/10.1016/j.compscitech.2006.10.021

[22] Hernández M., del Mar Bernal M., Verdejo R., Ezquerra T. A., López-Manchado M. A.: Overall performance of natural rubber/graphene nanocomposites. Composites Science and Technology, **73**, 40–46 (2012).
https://doi.org/10.1016/j.compscitech.2012.08.012

[23] Azizli M. J., Barghamadi M., Rezaeeparto K., Mokhtary M., Parham S.: Compatibility, mechanical and rheological properties of hybrid rubber NR/EPDM-*g*-MA/EPDM/graphene oxide nanocomposites: Theoretical and experimental analyses. Composites Communications, **22**, 100442 (2020).
https://doi.org/10.1016/j.coco.2020.100442

[24] Allahbakhsh A., Mazinani S.: Influences of sodium dodecyl sulfate on vulcanization kinetics and mechanical performance of EPDM/graphene oxide nanocomposites. RSC Advances, **5**, 46694–46704 (2015).
https://doi.org/10.1039/C5RA00394F

[25] Saravanan N., Rajasekar R., Mahalakshmi S., Sathishkumar T. P., Sasikumar K., Sahoo S.: Graphene and modified graphene-based polymer nanocomposites – A review. Journal of Reinforced Plastics and Composites, **33**, 1158–1170 (2014).
https://doi.org/10.1177/0731684414524847

[26] Potts J. R., Dreyer D. R., Bielawski C. W., Ruoff R. S.: Graphene-based polymer nanocomposites. Polymer, **52**, 5–25 (2011).
https://doi.org/10.1016/j.polymer.2010.11.042

[27] Gudarzi M. M., Sharif F.: Enhancement of dispersion and bonding of graphene-polymer through wet transfer of functionalized graphene oxide. Express Polymer Letters, **6**, 1017–1031 (2012).
https://doi.org/10.3144/expresspolymlett.2012.107

[28] Dash B. K., Achary P. G. R., Nayak N. C., Choudhary R. N. P.: Dielectric relaxation behavior of exfoliated graphite nanoplatelet-filled EPDM vulcanizates. Journal of Electronic Materials, **46**, 563–572 (2017).
https://doi.org/10.1007/s11664-016-4935-1

[29] Chang Y-W., Kim S., Kang S. C., Bae S-Y.: Thermomechanical properties of ethylene-propylene-diene terpolymer/organoclay nanocomposites and foam processing in supercritical carbon dioxide. Korean Journal of Chemical Engineering, **28**, 1779–1784 (2011).
https://doi.org/10.1007/s11814-011-0002-z

[30] Zhang H., Datta R. N., Talma A. G., Noordermeer J. W. M.: Maleic-anhydride grafted EPM as compatibilising agent in NR/BR/EPDM blends. European Polymer Journal, **46**, 754–766 (2010).
https://doi.org/10.1016/j.eurpolymj.2009.12.020

[31] Ismail H., Mathialagan M.: Curing characteristics, morphological, tensile and thermal properties of bentonite-filled ethylene-propylene-diene monomer (EPDM) composites. Polymer-Plastics Technology and Engineering, **50**, 1421–1428 (2011).
https://doi.org/10.1080/03602559.2011.584244

[32] Ismail H., Mathialagan M.: Compatibilization of bentonite filled ethylene-propylene-diene monomer composites: Effect of maleic anhydride grafted EPDM. Journal of Applied Polymer Science, **127**, 1164–1171 (2013).
https://doi.org/10.1002/app.37606

[33] Shaito A., Fairbrother D., Sterling J., D´Souza N. A.: Maleated amorphous ethylene propylene compatibilized polyethylene nanocomposites: Room temperature nonlinear creep response. Polymer Engeneering and Science, **50**, 1620–1632 (2010).
https://doi.org/10.1002/pen.21589

[34] Sirqueira A. S., Soares B. G.: The effect of functionalized ethylene propylene diene rubber (EPDM) on the kinetics of sulfur vulcanization of normal rubber/EPDM blends. Macromolecular Materials and Engineering, **292**, 62–69 (2007).
https://doi.org/10.1002/mame.200600332

[35] Correia C. A., Valera T. S.: Cellulose nanocrystals and jute fiber-reinforced natural rubber composites: Cure characteristics and mechanical properties. Materials Research, **22**, e20190192 (2019).
https://doi.org/10.1590/1980-5373-MR-2019-0192

[36] Sieradzka M., Ślusarczyk C., Fryczkowski R., Janicki J.: Insight into the effect of graphite grain sizes on the morphology, structure and electrical properties of reduced graphene oxide. Journal of Materials Research and Technology, **9**, 7059–7067 (2020).
https://doi.org/10.1016/j.jmrt.2020.05.026

[37] ASTM D2084-19: Standard test method for rubber property – Vulcanization using oscillating disk cure (2019).

[38] Flory P. J., Rehner J.: Statistical mechanics of cross-linked polymer networks I. Rubberlike elasticity. The Journal of Chemical Physics, **11**, 512–520 (1943).
https://doi.org/10.1063/1.1723791

[39] Mathew A. P., Packirisamy S., Radusch H. J., Thomas S.: Effect of initiating system, blend ratio and crosslink density on the mechanical properties and failure topography of nano-structured full-interpenetrating polymer networks from natural rubber and polystyrene. European Polymer Journal, **37**, 1921–1934 (2001). https://doi.org/10.1016/S0014-3057(01)00067-2

[40] ASTM D6814-02: Standard test method for determination of percent devulcanization of crumb rubber based on crosslink density (2019).

[41] Wypych G.: Handbook of polymers. ChemTec, Toronto (2012).

[42] Jacob M., Thomas S., Varughese K. T.: Mechanical properties of sisal/oil palm hybrid fiber reinforced natural rubber composites. Composites Science and Technology, **64**, 955–965 (2004). https://doi.org/10.1016/S0266-3538(03)00261-6

[43] ASTM D412-16: Standard test methods for vulcanized rubber and thermoplastic elastomers – Tension (2021).

[44] ASTM D1415-18: Standard test method for rubber property –7 International hardness (2018).

[45] Coran A. Y.: Vulcanization. Part VII. Kinetics of sulfur vulcanization of natural rubber in presence of delayed-action accelerators. Rubber Chemistry and Technology, **38**, 1–14 (1965). https://doi.org/10.5254/1.3535628

[46] Coran A. Y.: Chemistry of the vulcanization and protection of elastomers: A review of the achievements. Journal of Applied Polymer Science, **87**, 24–30 (2002). https://doi.org/10.1002/app.11659

[47] Coran A.: Blends of dissimilar rubbers—Cure-rate incompatibility. Rubber Chemistry and Technology, **61**, 281–292 (1988). https://doi.org/10.5254/1.3536188

[48] Stiehler R. D., Wakelin J. H.: Mechanism and theory of vulcanization. Industrial and Engineering Chemistry, **21**, 325–343 (1948). https://doi.org/10.5254/1.3546917

[49] Mensah B., Kumar D., Lim D-K., Kim S. G., Jeong B-H., Nah C.: Preparation and properties of acrylonitrile-butadiene rubber-graphene nanocomposites. Journal of Applied Polymer Science, **132**, 42457 (2015). https://doi.org/10.1002/app.42457

[50] Pasbakhsh P., Ismail H., Fauzi M. N. A., Bakar A. A.: Influence of maleic anhydride grafted ethylene propylene diene monomer (MAH-*g*-EPDM) on the properties of EPDM nanocomposites reinforced by halloysite nanotubes. Polymer Testing, **28**, 548–559 (2009). https://doi.org/10.1016/j.polymertesting.2009.04.004

[51] Iqbal S. S., Iqbal N., Jamil T., Bashir A., Khan Z. M.: Tailoring in thermomechanical properties of ethylene propylene diene monomer elastomer with silane functionalized multiwalled carbon nanotubes. Journal of Applied Polymer Science, **133**, 43221 (2016). https://doi.org/10.1002/app.43221

[52] Zheng H., Zhang Y., Peng Z., Zhang Y.: Influence of clay modification on the structure and mechanical properties of EPDM/montmorillonite nanocomposites. Polymer Testing, **23**, 217–223 (2004). https://doi.org/10.1016/S0142-9418(03)00097-7